

Supplementary Information

A Facile Grating Approach towards Broadband, Wide-angle and High-efficiency Holographic Metasurfaces

Zi-Lan Deng,^a Shuang Zhang^b and Guo Ping Wang^{*a}

^aCollege of Electronic Science and Technology and Key Laboratory of Optoelectronic Devices and Systems of Ministry of Education and Guangdong Province, Shenzhen University, Shenzhen 518060, China

^bSchool of Physics & Astronomy, University of Birmingham, Birmingham B15 2TT, UK.

*Email: gpwang@szu.edu.cn

I. The analytical model expansion theory

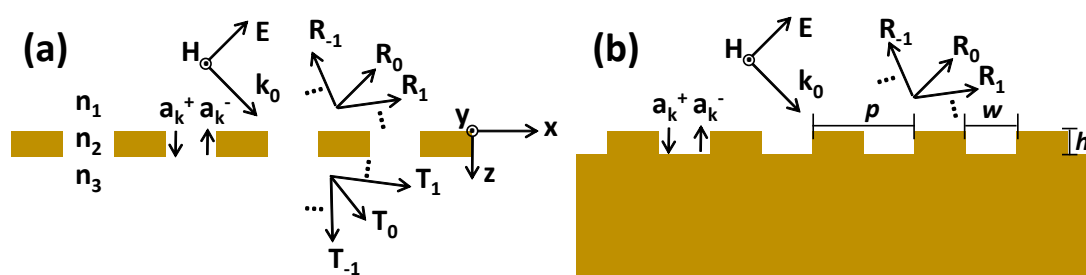


Fig. S1. Schematics of the (a) transmission and (b) reflection metallic grating. The excited k^{th} order cavity mode in gap areas is of upward and downward mode amplitudes a_k^{\pm} ($k = 0, 1, 2, \dots$). The refractive index in the upper layer, the gap area and the lower layer is $n_1 = \sqrt{\epsilon_1 \mu_1}$, $n_2 = \sqrt{\epsilon_2 \mu_2}$ and $n_3 = \sqrt{\epsilon_3 \mu_3}$ respectively.

Let's consider a general 3-layer medium as shown in Fig. S1. The metallic grating is

placed in the middle layer; the lower layer is dielectric/metal for transmission/reflection grating respectively. A transverse Magnetic (TM) plane wave illuminates the grating from the upper layer with arbitrary incident angle. There are multiple reflection and transmission diffraction orders governed by the grating equation. In the upper layer, the magnetic and electric field components can be written as,

$$H_{1y} = H_0 \left(e^{ik_{x0}x + ik_{z0}^{(1)}z} - \sum_{n=-\infty}^{\infty} R_n e^{ik_{xn}x - ik_{zn}^{(1)}z} \right), \quad (1a)$$

$$E_{1x} = \frac{1}{i\omega\epsilon_1\epsilon_0} \frac{\partial H_y}{\partial z} = \frac{k_{z0}^{(1)}H_0}{\omega\epsilon_1\epsilon_0} \left(e^{ik_{x0}x + ik_{z0}^{(1)}z} + \sum_{n=-\infty}^{\infty} R_n \frac{k_{zn}^{(1)}}{k_{z0}^{(1)}} e^{ik_{xn}x - ik_{zn}^{(1)}z} \right), \quad (1b)$$

where, $(k_{x0}, k_{z0}^{(1)} = \sqrt{n_1^2 k_0^2 - k_{x0}^2})$ is the wavevector of incident plane wave, and $(k_{xn} = k_{x0} + 2n\pi/p, k_{zn}^{(1)} = \sqrt{n_1^2 k_0^2 - k_{xn}^2})$ is the wavevector of the n^{th} diffraction order.

Considering the metal as perfect electric conductor (PEC), the field in the gap area can be written as the superposition of all the waveguide modes between the two metallic walls,¹

$$H_{2y} = H_0 \sum_{k=0}^{\infty} \cos\left(\frac{k\pi(x+w/2)}{w}\right) (a_k^+ e^{i\beta_k z} - a_k^- e^{-i\beta_k z}), \text{ for } (0 < z < h), \quad (2a)$$

$$E_{2x} = \frac{1}{i\omega\epsilon_2\epsilon_0} \frac{\partial H_y}{\partial z} = \frac{H_0}{\omega\epsilon_2\epsilon_0} \sum_{k=0}^{\infty} \beta_k \cos\left(\frac{k\pi(x+w/2)}{w}\right) (a_k^+ e^{i\beta_k z} + a_k^- e^{-i\beta_k z}), \text{ for } (0 \leq z \leq h), \quad (2b)$$

where, $\beta_k = \sqrt{n_2^2 k_0^2 - \left(\frac{k\pi}{w}\right)^2}$ is the propagation constant of the waveguide mode of the k^{th} order.

In the lower layer for the transmission grating, the field can be written as,

$$H_y = H_0 \sum_{n=-\infty}^{\infty} T_n e^{ik_{xn}x + ik_{zn}^{(3)}z}, \quad (3a)$$

$$E_x = \frac{1}{i\omega\epsilon_3\epsilon_0} \frac{\partial H_y}{\partial z} = \frac{k_{z0}^{(3)}H_0}{\omega\epsilon_3\epsilon_0} \sum_{n=-\infty}^{\infty} T_n \frac{k_{zn}^{(3)}}{k_{z0}^{(3)}} e^{ik_{xn}x + ik_{zn}^{(3)}z}, \quad (3b)$$

where, $k_{z0}^{(3)} = \sqrt{n_3^2 k_0^2 - k_{x0}^2}$, $k_{zn}^{(3)} = \sqrt{n_3^2 k_0^2 - k_{xn}^2}$.

The boundary condition at $z=0$ yields,

$$e^{ik_{x0}x} - \sum_{n=-\infty}^{\infty} R_n e^{ik_{xn}x} = \sum_{k=0}^{\infty} \cos\left(\frac{k\pi(x+w/2)}{w}\right) (a_k^+ - a_k^-), \quad (4a)$$

$$e^{ik_{x0}x} + \sum_{n=-\infty}^{\infty} R_n \frac{k_{zn}^{(1)}}{k_{z0}^{(1)}} e^{ik_{xn}x} = \frac{\varepsilon_1}{\varepsilon_2} \frac{1}{k_{z0}^{(1)}} \sum_{k=0}^{\infty} \beta_k \cos\left(\frac{k\pi(x+w/2)}{w}\right) (a_k^+ + a_k^-), \quad (4b)$$

and at $z=h$ for transmission grating, the boundary condition requires,

$$\sum_{n=-\infty}^{\infty} T_n e^{ik_{xn}x + ik_{zn}^{(3)}h} = \sum_{k=0}^{\infty} \cos\left(\frac{k\pi(x+w/2)}{w}\right) (a_k^+ e^{i\beta_k h} - a_k^- e^{-i\beta_k h}), \quad (5a)$$

$$\sum_{n=-\infty}^{\infty} T_n \frac{k_{zn}^{(3)}}{k_{z0}^{(3)}} e^{ik_{xn}x + ik_{zn}^{(3)}h} = \frac{\varepsilon_3}{\varepsilon_2} \frac{1}{k_{z0}^{(3)}} \sum_{k=0}^{\infty} \beta_k \cos\left(\frac{k\pi(x+w/2)}{w}\right) (a_k^+ e^{i\beta_k h} + a_k^- e^{-i\beta_k h}). \quad (5b)$$

Considering the orthogonality of different diffraction orders, we multiply Eq. (4b) and (5b) by $e^{-ik_{xn}x}$ and then integrate over $-p/2 < x < p/2$ respectively. It yields,

$$p\delta_{n0} + \frac{k_{zn}^{(1)}}{k_{z0}^{(1)}} pR_n = \frac{\varepsilon_1}{\varepsilon_2} \frac{1}{k_{z0}^{(1)}} \sum_{k=0}^{\infty} \beta_k (a_k^+ + a_k^-) \int_{-w/2}^{w/2} \cos\left(\frac{k\pi(x+w/2)}{w}\right) e^{-i(k_{x0} + 2n\pi/p)x} dx, \quad (6a)$$

$$\frac{k_{zn}^{(3)}}{k_{z0}^{(3)}} pT_n e^{ik_{zn}^{(3)}h} = \frac{\varepsilon_3}{\varepsilon_2} \frac{1}{k_{z0}^{(3)}} \sum_{k=0}^{\infty} \beta_k (a_k^+ e^{i\beta_k h} + a_k^- e^{-i\beta_k h}) \int_{-w/2}^{w/2} \cos\left(\frac{k\pi(x+w/2)}{w}\right) e^{-i(k_{x0} + 2n\pi/p)x} dx, \quad (6b)$$

As a result, R_n , T_n can be expressed in terms of a_k^+ , a_k^- as,

$$R_n = -\delta_{n0} + \frac{\varepsilon_1}{\varepsilon_2} \frac{1}{k_{zn}^{(1)} p} \sum_{k=0}^{\infty} \beta_k (a_k^+ + a_k^-) I_{kn}^-, \quad (7a)$$

$$T_n = e^{-ik_{zn}^{(3)}h} \frac{\varepsilon_3}{\varepsilon_2} \frac{1}{k_{zn}^{(3)} p} \sum_{k=0}^{\infty} \beta_k (a_k^+ e^{i\beta_k h} + a_k^- e^{-i\beta_k h}) I_{kn}^-. \quad (7b)$$

We multiply Eq. (4a) and (5a) by $\cos\left(\frac{k'\pi(x+w/2)}{w}\right)$ and use the orthogonality of waveguide modes of different orders, then integrate in terms of x in the region $-w/2 < x < w/2$ respectively, it yields,

$$I_{k'0}^+ = \sum_{n=-\infty}^{\infty} R_n I_{k'n}^+ + \frac{w}{2} (1 + \delta_{k'0}) (a_{k'}^+ - a_{k'}^-), \quad (8a)$$

$$0 = \sum_{n=-\infty}^{\infty} T_n e^{ik_{zn}^{(3)}h} I_{k'n}^+ - \frac{w}{2} (1 + \delta_{k'0}) (a_{k'}^+ e^{i\beta_k h} - a_{k'}^- e^{-i\beta_k h}). \quad (8b)$$

Substituting (7a) and (7b) into (8a) and (8b) respectively, it yields,

$$2I_{k'0}^+ = \frac{\varepsilon_1}{\varepsilon_2} \frac{1}{p} \sum_{k=0}^{\infty} \left[(a_k^+ + a_k^-) \beta_k \sum_{n=-\infty}^{\infty} \frac{I_{kn}^- I_{k'n}^+}{k_{zn}^{(1)}} \right] + \frac{w}{2} (1 + \delta_{k'0}) (a_{k'}^+ - a_{k'}^-), \quad (9a)$$

$$0 = \frac{\varepsilon_3}{\varepsilon_2} \frac{1}{p} \sum_{k=0}^{\infty} \left[(a_k^+ e^{i\beta_k h} + a_k^- e^{-i\beta_k h}) \beta_k \sum_{n=-\infty}^{\infty} \frac{I_{kn}^- I_{k'n}^+}{k_{zn}^{(3)}} \right] - \frac{w}{2} (1 + \delta_{k'0}) (a_{k'}^+ e^{i\beta_k h} - a_{k'}^- e^{-i\beta_k h}), \quad (9b)$$

where,

$$I_{kn}^- = \int_{-w/2}^{w/2} \cos\left(\frac{k\pi(x+w/2)}{w}\right) e^{-ik_{xn}x} dx = w \frac{-ik_{xn}w \left(\exp\left(\frac{1}{2}ik_{xn}w\right) - (-1)^k \exp\left(-\frac{1}{2}ik_{xn}w\right) \right)}{k_{xn}^2 w^2 - k^2 \pi^2} \quad (10a)$$

$$= \begin{cases} w \frac{2k_{xn}w \sin(k_{xn}w/2)}{k_{xn}^2 w^2 - k^2 \pi^2}, & k : \text{even} \\ w \frac{-2ik_{xn}w \cos(k_{xn}w/2)}{k_{xn}^2 w^2 - k^2 \pi^2}, & k : \text{odd} \end{cases}$$

$$I_{kn}^+ = \int_{-w/2}^{w/2} \cos\left(\frac{k\pi(x+w/2)}{w}\right) e^{ik_{xn}x} dx = w \frac{-ik_{xn}w \left((-1)^k \exp\left(\frac{1}{2}ik_{xn}w\right) - \exp\left(-\frac{1}{2}ik_{xn}w\right) \right)}{k_{xn}^2 w^2 - k^2 \pi^2} \quad (10b)$$

$$= \begin{cases} w \frac{2k_{xn}w \sin(k_{xn}w/2)}{k_{xn}^2 w^2 - k^2 \pi^2}, & k : \text{even} \\ w \frac{2ik_{xn}w \cos(k_{xn}w/2)}{k_{xn}^2 w^2 - k^2 \pi^2}, & k : \text{odd} \end{cases}$$

So far, the amplitude coefficients of the k^{th} ($k=0, 1, 2, \dots$) cavity mode a_k^{\pm} can be obtained by solve the linear equations defined by Eq. (9). Finally, substituting the solved amplitude coefficients back into Eqs. (7), we can readily obtain the reflection and transmission coefficients of arbitrary diffraction orders.

For the reflection grating as shown in Fig. S1b, the situation becomes much simpler. The boundary condition at $z=h$ is simply $E_x=0$, which yields

$a_k^+ e^{i\beta_k h} + a_k^- e^{-i\beta_k h} = 0$. As a result, the downward amplitude coefficient a_k^- can be directly written in terms of the upward amplitude coefficient a_k^+ ,

$$a_k^- = -a_k^+ e^{2i\beta_k h}, \quad (11)$$

substituting it into (7a) and (9a) respectively, it yields,

$$R_n = -\delta_{n0} + \frac{\varepsilon_1}{\varepsilon_2} \frac{1}{k_{zn}^{(1)} p} \sum_{k=0}^{\infty} a_k^+ \beta_k (1 - e^{2i\beta_k h}) I_{kn}^-, \quad (12)$$

$$2I_{k'0}^+ = \frac{\varepsilon_1}{\varepsilon_2} \frac{1}{p} \sum_{k=0}^{\infty} \left[a_k^+ (1 - e^{2i\beta_k h}) \beta_k \sum_{n=-\infty}^{\infty} \frac{I_{kn}^- I_{kn}^+}{k_{zn}^{(1)}} \right] + \frac{w}{2} (1 + \delta_{k'0}) (1 + e^{2i\beta_{k'} h}) a_{k'}^+. \quad (13)$$

Now, we need only solve the upward amplitude coefficient a_k^+ ($k=0, 1, 2, \dots$) for each cavity mode by Eq. (13), and substitute a_k^+ back into Eq. (12) to obtain the reflection coefficients for arbitrary diffraction orders.

For the grating with ultra-narrow grooves ($w \ll \lambda/2$), only the fundamental cavity mode ($k=0$) is supported while the higher modes are cut-off, thus we can explicitly write the mode amplitude coefficient and reflection coefficient of the n^{th} diffraction order as,

$$a_0^+ = \frac{2 \sin c(k_{x0} w / 2)}{(1 + e^{2in_2 k_0 h}) + (1 - e^{2in_2 k_0 h}) \frac{\varepsilon_1 w}{\varepsilon_2 p} \sum_{n'=-\infty}^{\infty} \frac{n_2 k_0}{k_{zn'}} \sin c^2 \left(\frac{k_{xn'} w}{2} \right)}, \quad (14)$$

$$R_n = -\delta_{n0} - \frac{i 2 \tan(n_2 k_0 h) \frac{n_2 k_0}{k_{zn}^{(1)}} \frac{\varepsilon_1 w}{\varepsilon_2 p} \sin c \left(\frac{k_{x0} w}{2} \right) \sin c \left(\frac{k_{xn} w}{2} \right)}{1 - i \tan(n_2 k_0 h) \frac{\varepsilon_1 w}{\varepsilon_2 p} \sum_{n'=-\infty}^{\infty} \frac{n_2 k_0}{k_{zn'}} \sin c^2 \left(\frac{k_{xn'} w}{2} \right)}. \quad (15)$$

For the grating with broad groove width ($w/p \sim 0.5$), in our interesting wavelength range, only the first two cavity modes ($k=0, 1$) are not cut-off. As a result, we only need to solve a 2×2 matrix to obtain a_0^+ and a_1^+ , and then substitute them into Eq. (12) to obtain the reflection coefficient of k^{th} order as follows,

$$R_n = -\delta_{n0} + \frac{\varepsilon_1}{\varepsilon_2} \frac{w}{k_{zn}^{(1)} p} \left[a_0^+ \beta_0 (1 - e^{2i\beta_0 h}) \operatorname{sinc} \left(\frac{k_{xn} w}{2} \right) - a_1^+ \beta_1 (1 - e^{2i\beta_1 h}) \frac{2ik_{xn} w \cos(k_{xn} w / 2)}{k_{xn}^2 w^2 - \pi^2} \right]. \quad (16)$$

II. Comparison between extraordinary optical transmission and diffraction.

Based on the analytic model theory in part I, we plot the transmittances and reflectances of different diffraction orders for a large range of incident angle and wavevector in Fig. S2. We can split the (θ_0, k_0) plane into multiple subregions by the Rayleigh anomaly (RA) curves defined by,

$$k_0 \sin \theta_0 + 2n\pi / p = \pm k_0, \quad n = \pm 1, \pm 2, \dots, \quad (17)$$

which are automatically shown by the abrupt color changes as labeled in Fig. S2d. By varying the grating height, we can tune the resonance of the cavity mode in different subregions. When $2h=0.7$ for the transmission grating (Fig. S2a-S2c), the lowest resonance of the cavity mode happens in the most left-down subarea, where only T_0 and R_0 channel are allowed to propagate in free-space. The resonance leads to the total suppression of R_0 (blue-dip in the most left-down subregion in Fig. S2a) and enhancement of T_0 (red-peak in the most left-down subregion in Fig. S2b). The resonance transmission is referred to as the well-known extraordinary optical transmission (EOT) phenomenon which is widely studied in the past decades². By decreasing h to 0.25 and adopting the reflection grating geometry (Fig. S2d-S2f), the resonance shifts to the second lower subregion where only -1^{st} , and 0^{th} reflections are allowed to propagate (the white numbers denoted in Fig. S2d). Similarly, the resonance suppresses the ordinary specular reflection R_0 , while enhances the -1^{st} reflection R_{-1} to unity. And we refer to such resonance phenomenon as extraordinary

optical diffraction (EOD). By further decreasing the height, the cavity mode resonance will shift to subregions with higher diffraction orders. For $h=0.15$ (Fig. S2h-S2j), the resonance extends to the subregion bounded by 1st, -2nd and -3th RA curves. In this subregion, there exist the 0th, -1st and -2nd propagating channels. The 0th reflection is again totally suppressed, but the R_{-2} is not enhanced to unity due to the coexistence with R_{-1} . Instead, the efficiency for R_{-2} and R_{-1} are both enhanced to about 0.5 as shown Fig. S2j.

Note that, we can't enhance $-n^{\text{th}}$ ($n>1$) diffraction order to 100% by the cavity mode resonance since when $-n^{\text{th}}$ diffraction order is propagating, the lower orders (-1st, -2nd, ..., $-(n-1)^{\text{th}}$) are also allowed to propagate (Fig. S2d) and we can't find a subregion where there are and only are the 0th and $-n^{\text{th}}$ ($n>1$) propagating diffraction orders.

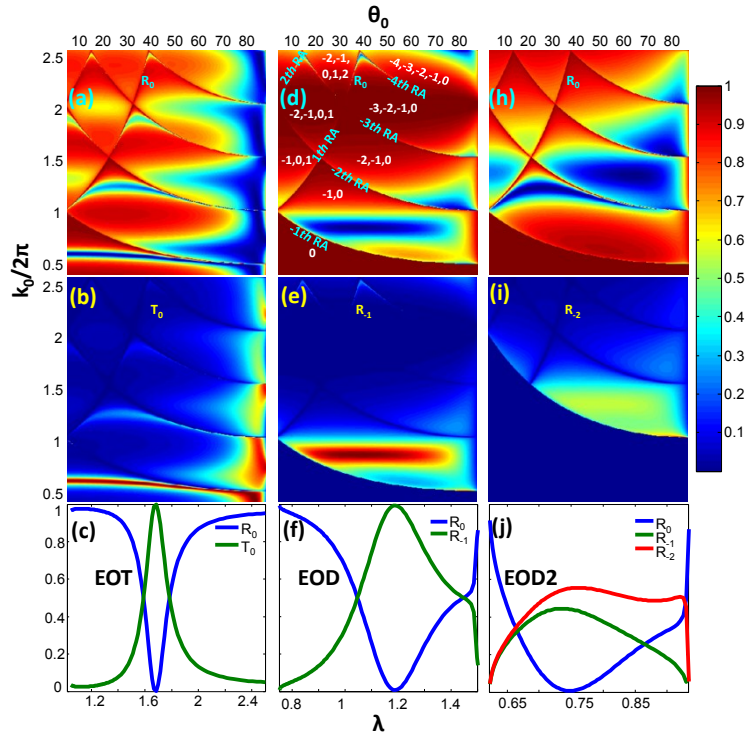


Fig. S2. The evolution from EOT to EOD by simply varying the resonance position of

the cavity mode. (a-c) show the EOT for transmission grating with $2h=0.7$. The cavity mode resonance locates below the -1^{st} RA, where only 0^{th} diffraction order is allowed to propagate. R_0 is suppressed while T_0 is enhanced on resonance. (d-f) show the EOD for reflection grating with $h=0.25$. The cavity mode resonance locates in the subregion where only the 0^{th} and -1^{st} reflections is allowed. R_0 is completely suppressed while R_{-1} is enhanced to unity on resonance. (h-j) show the case when we further shift the resonance to higher frequencies ($h=0.15$) where the -2^{nd} , -1^{st} and 0^{th} reflections are allowed. R_0 is totally suppressed while R_{-1} and R_{-2} are simultaneously enhanced to about 0.5 respectively. The first and second row show the specular reflectance R_0 and the diffraction efficiency for a particular order: (b) T_0 , (e) R_{-1} , and (i) R_{-2} respectively with varying incident angle and wavevector. The last row show the spectra with a particular incident angle (c) 0° , (f) 30° , and (j) 60° for the corresponding grating.

III. The origin of the broadband high diffraction efficiency

It is well known that, the effect based on resonance is always of narrow bandwidth. The EOD due to CM also has a narrow bandwidth for small gap width. One can increase the gap width w to reduce the resonance strength to obtain a relatively broad bandwidth, but solely one CM can't lead to a flat-top high efficiency for R_{-1} as shown in Fig. S3a-S3b. At the same time, the CM_1 emerges when w is increased to $0.5p$. By only considering the contribution of CM_1 (a_1^\pm), the narrow resonance of CM_1 will lead to the peak (dip) of R_{-1} (R_0). In the real system, CM_0 and CM_1 coexist. The interference between the broad CM_0 and narrow CM_1 leads to an asymmetry Fano lineshape near $\lambda=0.82$ (Fig. S3f). As CM_1 is located in the marginal position of CM_0 , the Fano interference will push up R_{-1} for $\lambda>0.82$, while pull down R_{-1} sharply for λ slightly <0.82 . As a result, a flat-top shape of R_{-1} is formed as shown by the solid green curve in Fig. S3f.

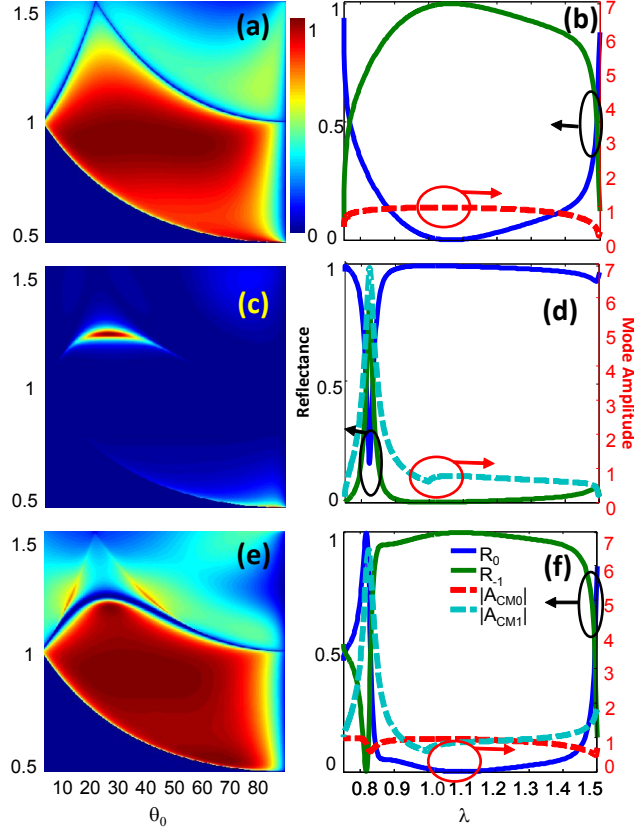


Fig. S3 The reflection spectra calculated by considering the contribution of (a, b) only the CM_0 , (c, d) only the CM_1 and (e, f) both CM_0 and CM_1 respectively.

IV. Modulation range of extraordinary optical diffraction.

The EOD can happen for a large range of incident angle and wavelength when the duty-cycle is near $w/p \approx 0.5$. In order to realize the wavefront shaping, we should have a large modulation range of phase. For a usual metasurface, people always look for a full phase modulation range ($0-2\pi$) by changing the shape or size of the unit-cell structure. Here, in our holographic metasurface based on mode cavity resonance, we do not modulate phase directly, but modulate the phase gradient by the grating period. If a wavefront has steep phase gradient profile, we require a large range of applicable period to shape such complex wavefront. From Fig. S4a, we see that for a fix wavelength, the -1^{st} reflectance can reach unity for a large range of p and incident

angle. The available range of p is only restricted by the -1st RA and the high order (1st) resonance of cavity mode. At a specified incident angle (Fig. S4b), we can clearly see the flat-top reflectance of -1st order with respect to p , allowing us to modulate the phase of complex wavefront with high conversion efficiency. For the realistic silver grating operating at visible frequencies (Fig. S4c and S4d), the period range for high -1st diffraction is still survival, although the bandwidth is narrow than the PEC grating due to the much lower resonance of CM₁. For example, in the grating with carrier period 424nm, operating wavelength 600nm and incident angle $\theta_0=45^\circ$, the bandwidth for diffraction efficiency over 90% can be obtained as 375nm to 500nm (green curve, Fig. S4d).

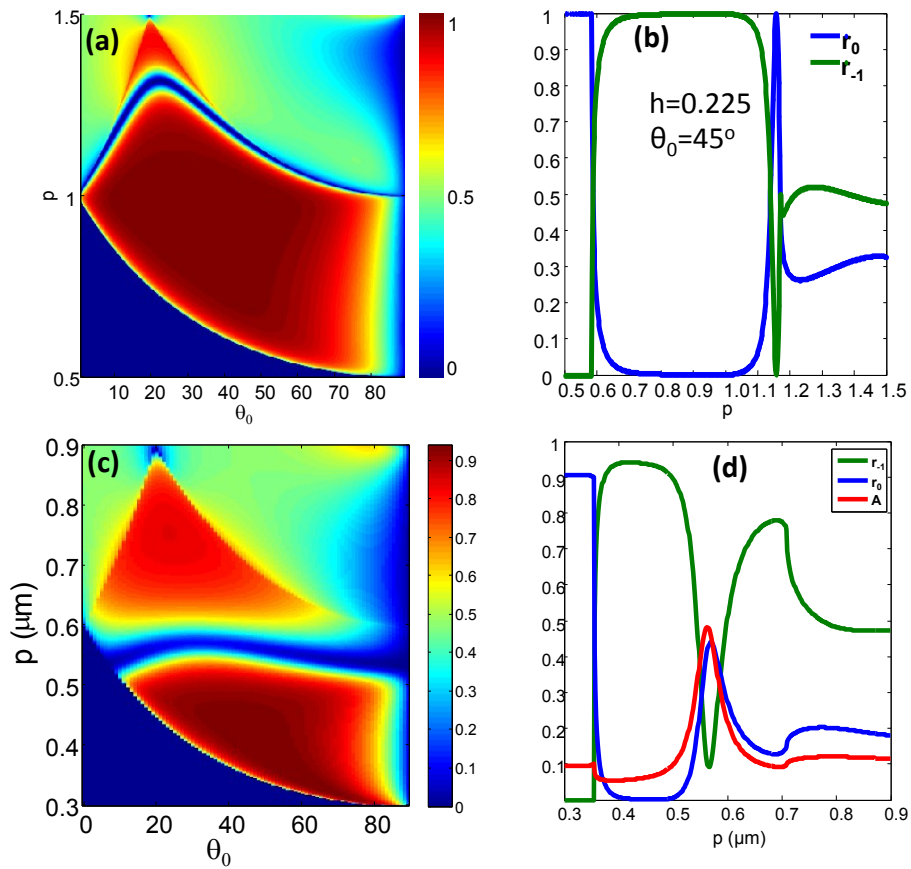


Fig S4. The applicable range of grating period p for EOD. (a) The -1st reflectances with varying incident angle θ_0 and grating period p for PEC grating with height

$h=0.225$, fixed duty cycle 0.5 and fixed working wavelength $\lambda=1$. (b) The 0th and -1st reflectances as a function of p at the vertical cut at $\theta_0=45^\circ$ in (a). There is a wide flat-top range of R_{-1} from $p=0.7$ to 1.05, allowing for a large range of phase modulation and thus promising the shaping of complex wavefront with high efficiency. (c) The -1st reflectances with varying incident angle θ_0 and grating period p for silver grating with height 130nm, fixed duty cycle 0.5 and fixed working wavelength $\lambda=600\text{nm}$. (d) The 0th and -1st reflectances and the absorption A as a function of p at the vertical cut at $\theta_0=45^\circ$ in (c). There is a wide flat-top range from $p=375\text{nm}$ to 500nm for -1st reflectance over 90%.

V. Extraordinary optical diffraction due to excitation of high order cavity modes.

Besides the lowest order resonance, high order resonances of the cavity mode also can lead to extraordinary total reflection in the -1st diffraction order as shown in Fig. S5. The n^{th} resonance of cavity mode happens when the groove height is a little smaller than the n^{th} Fabry-Perot resonance condition $h \sim (n+1/2)\lambda/2$. The incident light will be completely reflected in the -1st diffraction channel for those groove heights as shown in Fig. S5d-S5f. Instead, for the off-resonance case with $h=n\lambda/2$, the incident light will go to the ordinary specular reflection path as shown in Fig. S5h-S5j. However, the band width for high order resonances are intrinsically narrower than the 0th order resonance (Fig. S5a-S5c). Moreover, the required large groove height for high order resonance makes the fabrication much more difficult. Therefore the lowest resonance of cavity mode is the optimal condition for EOD.

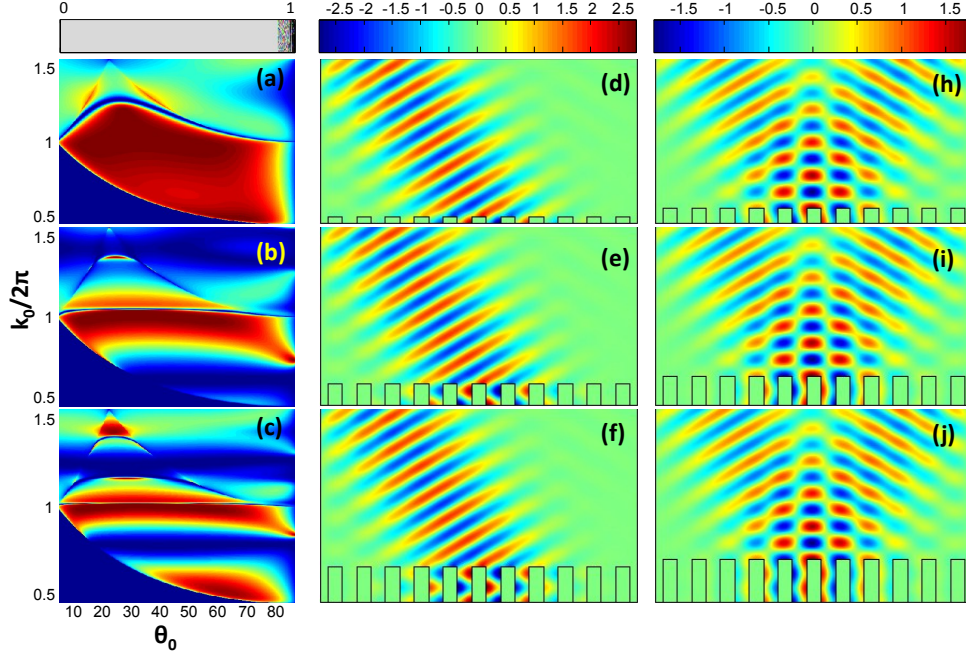


Fig. S5. EOD due to high order resonances of cavity mode. (a-c) are the -1st reflectance with varying incident angle θ_0 and wavevector k_0 for different groove height: (a) $h=0.225$, (b) $h=0.725$, (c) $h=1.225$. (d-f) show the corresponding field patterns (H_y) at the (d) 0th ($h=0.225$), (e) 1st ($h=0.725$), and (f) 2nd ($h=1.225$) resonance respectively. For comparison, (h-j) show the field patterns for off resonance at different height: (h) $h=0.5$, (i) $h=1$, and (j) $h=1.5$ respectively. The grating period and groove width in (a-j) are $p=1$ and $w=0.5$ respectively. The wavelength and incident angle in (d-j) are $\lambda=1$ and $\theta_0=30^\circ$ respectively.

VI. Extraordinary optical diffraction for real metal in different frequency range.

In the analytic model expansion theory, the metal is considered as PEC, which is a good approximant of real metal in lower frequency band such as mid-infrared, Terahertz and Microwave range. In the optical frequency range, the dispersion and loss of metal will play a significant role. However, we can still obtain similar conclusions by simulating the reflectances of different diffraction orders with the Rigorous Coupled Wave Analysis (RCWA) method. Using the geometry parameters predicted by analytic model, we can still obtain a relatively broad dip for R_0 and a broad peak for R_{-1} , as shown in Fig. S6. The peak value of R_{-1} can't reach unity due to

the metallic loss. However, it can also reaches value as high as 0.95. And there is still a wide-angle range for EOD. The -1^{st} reflectance for grating operating in the near-infrared range ($1\mu\text{m}\sim 3\mu\text{m}$) is almost the same as the PEC results (Fig. S3e). When we increase the working frequencies ($0.5\mu\text{m}\sim 1.5\mu\text{m}$ in Fig. S6b), the position of CM_1 will shift to lower frequencies, leading to a decrease of the upper bound of the bandwidth. It is because the real metal has finite skin depth, the cavity mode resonance will be replaced by the localized gap surface plasmon resonance. The propagating constant of the gap surface plasmon is greater than that of the PEC waveguide mode.

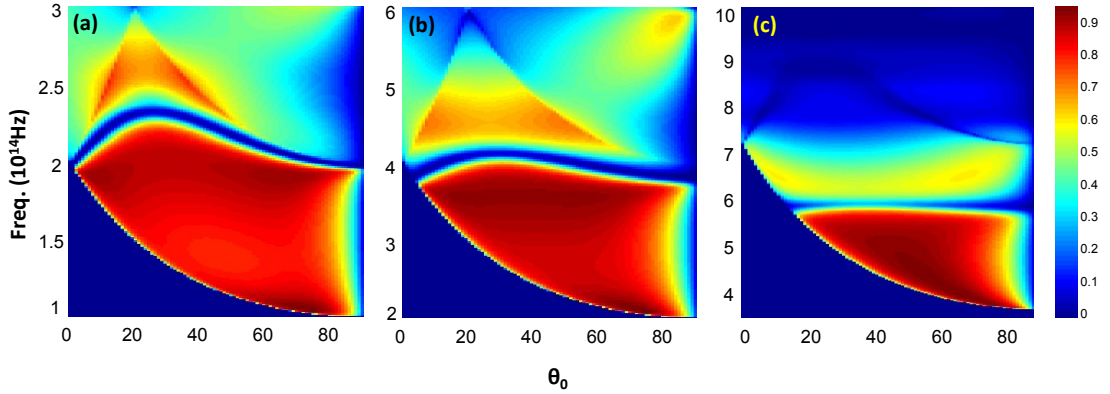


Fig. S6. -1^{st} reflectance with varying incident angle θ_0 and frequencies for metallic reflection grating in optical frequencies calculated by RCWA. The parameters for the grating are (a) $p=1.5\mu\text{m}$, $w=750\text{nm}$, and $h=337.5\text{nm}$; (b) $p=750\text{nm}$, $w=375\text{nm}$, $h=202.5\text{nm}$; (c) $p=424\text{nm}$, $w=212\text{nm}$, $h=130\text{nm}$. The metal is considered as silver, whose refractive index is taken from the experimental data.³

VII. Extraordinary optical diffraction due to excitation of propagating surface plasmon polaritons.

For the EOD due to excitation of cavity mode, the groove height should be thick enough so as to support the cavity mode in the vertical direction. For metallic grating with shallow groove height, the propagating surface plasmon mode will be excited

when the parallel wavevector of incident light plus the grating's reciprocal lattice vector matches the propagating constant of the surface plasmon mode k_{spp} ,

$$\begin{aligned} k_0 \sin \theta_0 + n \frac{2\pi}{p} &= k_{spp} \quad (n > 0) \\ k_0 \sin \theta_0 + n \frac{2\pi}{p} &= -k_{spp} \quad (n < 0) \end{aligned} \quad (18)$$

In Fig. S7a and S7b, the surface plasmon modes near the 1st ($\sin \theta_0 = \frac{k_{spp}}{k_0} - \frac{\lambda}{p}$) and -

2nd ($\sin \theta_0 = \frac{2\lambda}{p} - \frac{k_{spp}}{k_0}$) RA are excited. Since k_{spp} is a little larger than k_0 , the surface

plasmon resonance is slightly below the 1st and -2nd RA curve (red peak curve in Fig. S7b). Thereby, those surface plasmon resonances are just inside the subarea where

only R_0 and R_{-1} are the allowed propagating channels. As a result, R_0 is suppressed while R_{-1} is enhanced at the surface plasmon resonances. Note that, due to the

inevitable loss of metal, there are strong absorptions at the surface plasmon resonances (Fig. S7c), which will decrease the peak value of R_{-1} to about 0.5. The

surface plasmon modes just below the -1st RA ($\sin \theta_0 = \frac{\lambda}{p} - \frac{k_{spp}}{k_0}$) are also excited.

Those surface plasmon resonances lead to the perfect absorption (red peak in the left-down corner of Fig. S7c) as reported previously,⁴ because only R_0 is the only

propagating channel in this subarea. Figure S7 d-S7f show the field patterns at the red peaks in Fig. S7b for different incident angles. We can clearly see the surface plasmon

wave in the metal-air interface, which further proves that the enhancement of R_{-1} indeed is due to the excitation of the propagating surface plasmon mode. Note that,

the EOD due to propagating surface plasmon is strongly dependent on incident angle

and the bandwidth is ultra-narrow. Thereby, it is not desirable for wide-angle and broad band wavefront shaping. It may be used in other areas such as sensing and switching applications which require sharp and angle-sensitive characteristics.

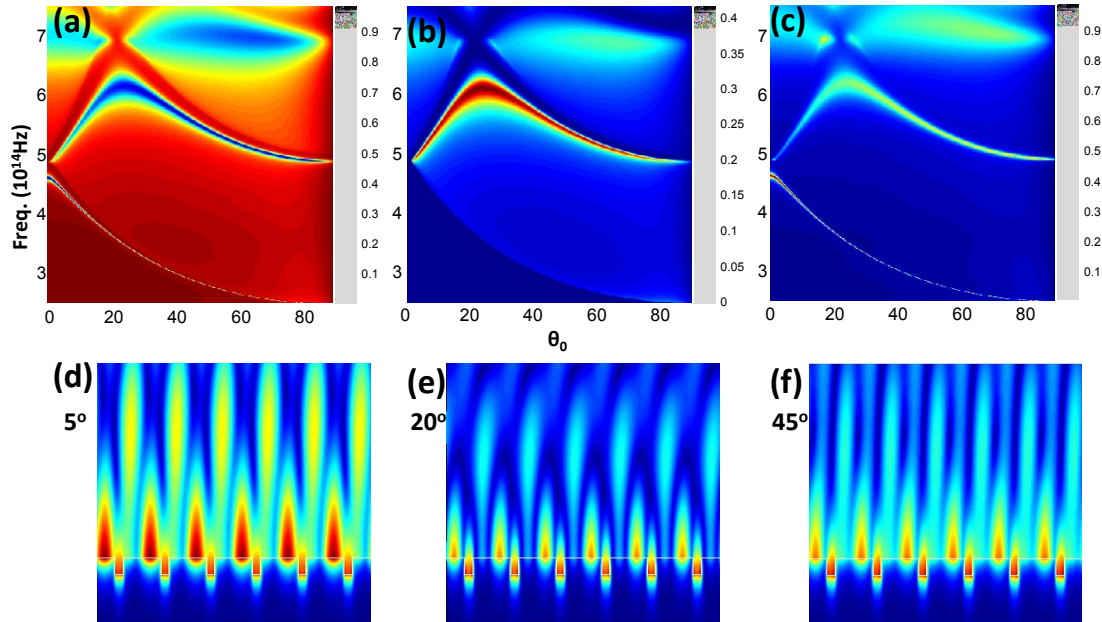


Fig. S7. The (a) 0th, (b) -1st order reflectance and (c) absorption with varying incident angle θ_0 and frequencies for metallic reflection grating with shallow groove height calculated by RCWA. The parameters for the grating are $p=600\text{nm}$, $w=100\text{nm}$, and $h=30\text{nm}$ respectively. The metal is considered as silver whose refractive index is taken from the experimental data ³. The lower panel show the field patterns ($|H_y|^2$) at the R_{-1} peak for different incident angle and wavelength: (d) 5°, 586nm, (e) 20°, 500nm and (f) 45°, 540nm.

References

1. J. A. Kong, *Electromagnetic wave theory*, EMW Publishing, Cambridge, 2008.
2. J. A. Porto, F. J. García-Vidal and J. B. Pendry, *Phys. Rev. Lett.*, 1999, **83**, 2845-2848.
3. E. D. Palik, *Handbook of Optical Constants of Solids*, Academic Press, San Diego, 1998.
4. Y. Cui, Y. He, Y. Jin, F. Ding, L. Yang, Y. Ye, S. Zhong, Y. Lin and S. He, *Laser Photonics Rev.*, 2014, **8**, 495-520.